Replacement of Val3 in Human Thymidylate Synthase Affects Its Kinetic Properties and Intracellular Stability[†,‡]

Xiao Huang,[§,#] Lydia M. Gibson,[§,#] Brittnaie J. Bell,[§] Leslie L. Lovelace,[§] Maria Marjorette O. Peña,[‖,@]
Franklin G. Berger,[‖,@] Sondra H. Berger,[@,⊥] and Lukasz Lebioda*[§,@]

[§]*Department of Chemistry and Biochemistry,* [‖]*Department of Biological Sciences,* [⊥]*Department of Pharmaceutical and Biomedical Sciences, and* [@]*Center for Colon Cancer Research, University of South Carolina, Columbia, South Carolina 29208.*
[#]*These authors contributed equally to this work.*

ABSTRACT: Human and other mammalian thymidylate synthase (TS) enzymes have an N-terminal extension of ∼27 amino acids that is not present in bacterial TSs. The extension, which is disordered in all reported crystal structures of TSs, has been considered to play a primary role in protein turnover but not in catalytic activity. In mammalian cells, the variant V3A has a half-life similar to that of wild-type human TS (wt hTS) while V3T is much more stable; V3L, V3F, and V3Y have half-lives approximately half of that for wt hTS. Catalytic turnover rates for most Val3 mutants are only slightly diminished, as expected. However, two mutants, V3L and V3F, have strongly compromised dUMP binding, with $K_{m,app}$ values increased by factors of 47 and 58, respectively. For V3L, this observation can be explained by stabilization of the inactive conformation of the loop of residues 181−197, which prevents substrate binding. In the crystal structure of V3L, electron density corresponding to a leucine residue is present in a position that stabilizes the loop of residues 181−197 in the inactive conformation. Since this density is not observed in other mutants and all other leucine residues are ordered in this structure, it is likely that this density represents Leu3. In the crystal structure of a V3F·FdUMP binary complex, the nucleotide is bound in an alternative mode to that proposed for the catalytic complex, indicating that the high $K_{m,app}$ value is caused not by stabilization of the inactive conformer but by substrate binding in a nonproductive, inhibitory site. These observations show that the N-terminal extension affects the conformational state of the hTS catalytic region. Each of the mechanisms leading to the high $K_{m,app}$ values can be exploited to facilitate design of compounds acting as allosteric inhibitors of hTS.

Thymidylate synthase (TS)[1] is the essential enzyme that catalyzes the formation of dTMP from dUMP, using 5,10-methylenetetrahydrofolate (mTHF) as a cosubstrate (*1*). The reaction is initiated by the active site cysteine, Cys195 in human TS (hTS), attacking C6 of dUMP. This leads to the formation of a covalent bond between TS and dUMP as well as activation of C5 of dUMP, generating a second covalent bond between dUMP and mTHF and ultimately a ternary catalytic complex. This reaction is the only de novo source of intracellular dTMP, although the thymidine salvage pathway may function as an alternative extracellular source of dTMP (*2*). Inhibition of hTS in

rapidly dividing cells leads to nucleotide imbalance and ultimately results in apoptosis. For this reason, TS has been an important target in the chemotherapy of colon cancer and some other malignancies.

hTS is a homodimer of 313 amino acids, and in general, the TS amino acid sequences are very highly conserved. The major differences between mammalian TSs and those from bacterial sources are an N-terminal extension of approximately 25−29 amino acids and two insertions of 12 and 8 residues at positions 117 and 145, respectively (*2*). Unlike the sequence in the catalytic part of the molecule, the sequence of the N-terminal extension is poorly conserved. X-ray crystallography of the rat and human TS enzymes has shown that this region is intrinsically disordered (*3−6*). Although extensive sequence divergence has occurred during the evolution of the N-terminal regions of TS polypeptides in mammalian species, a disordered structure with a high proline content and high frequency of disorder-promoting residues compared to the rest of the TS molecule has been conserved. Also, a Pro residue at the penultimate site is conserved in all species examined with the exception of mouse TS (*7*).

The N-terminal extension has been shown to play an important role in determining the intracellular stability of hTS and to control its degradation. Biochemical and genetic evidence indicates that degradation of the hTS polypeptide is conducted by the 26S proteasome but does not require ubiquitinylation or the

*To whom correspondence should be addressed: Department of Chemistry and Biochemistry, University of South Carolina, Columbia, SC 29208. Phone: (803) 777-2140. Fax: (803) 777-9521. E-mail: lebioda@mail.chem.sc.edu.
[1]Abbreviations: TS, thymidylate synthase; hTS, human TS; FdUMP, 5-fluoro-2′-deoxyuridine monophosphate; dUMP, 2′-deoxyuridine 5′-monophosphate; dTMP, 2′-deoxythymidine 5′-monophosphate; CH_2H_4folate or mTHF, 5,10-methylenetetrahydrofolate; EDTA, ethylenediaminetetraacetic acid; BME, β-mercaptoethanol; PDPA, 1,3-propanediphosphonic acid; PDB, Protein Data Bank; PEG, polyethylene glycol; rmsd, root-mean-square deviation.

ubiquitinylation pathway (*8*). The N-terminal region, in particular, the first 29 disordered residues, directs the protein to the ubiquitin-independent degradation pathway (*8, 9*). Deletion of the first two to six residues results in very stable enzymes with half-lives of >48 h. In addition, single-amino acid substitutions at the penultimate site, Pro2, have a profound impact on the half-life of the enzyme (*8, 9*). Previous studies by Edman degradation experiments showed that the primary sequence of hTS begins with an unblocked Pro residue, indicating that the protein undergoes posttranslational modification by Met excision (*10*). Analyses of hTS mutants with substitutions at Pro2 by MALDI-TOF showed that unstable mutants such as those with P2V and P2A substitutions undergo Met excision. On the other hand, stable mutants such as those in which Pro2 has been replaced with the remaining amino acids undergo either N^α-acetylation or both Met excision and N^α-acetylation, resulting in a blocked N-terminus (*7*). These results suggest that a free, unblocked N-terminus is a requisite for efficient degradation of hTS by the proteasome. Modifications such as N^α-acetylation might stabilize the enzyme by hindering its ability to efficiently recognize and/or enter the proteasomal chamber (*7*).

The role of the N-terminus in directing protein degradation is underscored by its ability to destabilize *Escherichia coli* TS (ecTS). This enzyme lacks the N-terminal extension and has a half-life of >48 h in mammalian cells. Fusion of the first 29 amino acids of hTS to the N-terminus of the ecTS reduced its half-life to <4 h (*9*). Furthermore, fusion of the first 45 amino acids, which includes the disordered region and the adjacent α-helix of hTS, to the enhanced green fluorescent protein (eGFP) destabilized this structurally unrelated protein from a half-life of >48 h to a half-life of ~7 h (*7*). Mutations in the N-terminus that affect the half-life of hTS exerted the same effects on the half-life of the N-terminal fusions with ecTS and eGFP, indicating that this region functions as a degron by promoting the degradation of an unrelated protein to which it is fused (*7, 9*).

A unique feature of hTS is the existence of the loop of residues 181−197 (loop 181−197) in two conformations (*3, 4*). One is similar to those found in TS enzymes from other sources and in complexes of hTS with substrate analogues (*11*); it is termed the "active conformation". In the second "inactive" conformation, loop 181−197 is flipped 180° and the catalytic Cys195 is located outside the active site (*4*), making the enzyme inactive. Studies of conformational switching in solution indicated that the two conformations are represented to a similar extent and that binding of dUMP shifts the equilibrium toward the active conformation while binding of phosphate or sulfate ions shifts the equilibrium toward the inactive conformation (*3*). Crystallization of TS proteins is facilitated by the presence of phosphate or sulfate ions; therefore, all crystal structures of native wild-type (wt) hTS are in the inactive conformation. Two crystallization conditions that yielded good crystals of hTS are 1.8−2.0 M ammonium sulfate (AS) (*12*) and a relatively low ionic strength, 30 mM AS, with polyethylene glycol (PEG) as the precipitant (*13*).

In the native hTS structure obtained at a low AS concentration (inactive conformer), electron density consistent with a *tert*-butyl moiety was observed (*13*). This density is likely from a valine or a leucine from a disordered region, and the corresponding residue interacts with a hydrophobic pocket that includes Trp182 and Leu187 from loop 181−197. The disordered regions in the structure correspond to the N-terminal extension, which contains Val3, and loop 108−129, which contains Leu118 and Leu121.

The hydrophobic interactions between the *tert*-butyl group and loop 181−197 must stabilize the inactive conformer. A hTS variant, missing residues 7−29, crystallized with loop 181−197 in the active conformation under very similar crystallization conditions with 50 mM phosphate (*14*). Thus, the Δ7−29 deletion affects the conformation of loop 181−197. It appeared likely that this effect is mediated by Val3, and an expansion of the *tert*-butyl moiety into a strongly binding ligand should generate an allosteric inhibitor of hTS. We report here studies of hTS variants at position 3 which confirm the Val3 hypothesis.

MATERIALS AND METHODS

Bacterial Strains and Plasmids. *E. coli* strain TX61⁻ (thyA⁻) and the pTS080 plasmid, expressing wt hTS, were generously provided by W. S. Dallas (Glaxo Wellcome, Research Triangle Park, NC) and have been described previously (*15, 16*). pTS080 contains resistance genes for ampicillin and tetracycline. TX61⁻ is a *thy*⁻ kanamycin-resistant mutant of BL21(DE3) and lacks detectable TS activity (*15*). For propagation, pTS080 was transformed into competent JM109 bacterial cells and grown in LB medium containing 50 µg/mL tetracycline. Plasmid DNA was isolated using the Qiagen Plasmid prep kit according to the manufacturer's instructions. Plasmid pJZ205 containing the hTS cDNA under the control of the SV40 promoter has been described previously (*17*) and was propagated in the DH5-α bacterial strain.

Cells and Cell Culture. The RJK88.13 cell line, which is a TS-deficient derivative of V79 Chinese hamster lung cells, was obtained from R. Nussbaum (University of Pennsylvania, Philadelphia, PA). These cells were maintained in Dulbecco's modified Eagle's medium (Cellgro) containing 4.5 g/L glucose and supplemented with 10% heat-inactivated fetal bovine serum (Cellgro) and 10 µM thymidine. Cells were cultured at 37 °C in a humidified 5% CO_2 atmosphere. To determine half-lives of TS mutants, cycloheximide (50 µg/mL, Sigma Aldrich) was added to growing cells followed by harvest at the indicated time points.

Site-Directed Mutagenesis. The mutagenic primers were designed to be complementary to the sense strand of human TS cDNA. Mutagenic primers were synthesized and purified by Integrated DNA Technology (IDT, Coralville, IA). Site-directed mutagenesis was performed using the Quick Change method (Stratagene, La Jolla, CA) with modifications as described previously (*17*). Mutations were confirmed by LiCor DNA sequence analysis (MUSC Biotechnology Resource Laboratory, Charleston, SC) of the entire TS gene. Plasmids containing the correct mutations were transformed into the TX61⁻ bacterial strain and screened successively on LB plates containing 50 µg/mL tetracycline and 40 µg/mL kanamycin. Colonies were picked from the kanamycin plates, grown in 5 mL of LB containing 50 µg/mL tetracycline, and used to make cell stocks for protein expression and purification.

For expression of Val3 mutants in RJK88.13 cells, plasmid pJZ205 was used as a template for mutagenesis as described above. Sequences of primers used to create V3A, V3T, V3L, V3Y, and V3F substitutions at codon 3 are available upon request. Following verification of mutations by sequencing, plasmids were stably transfected into TS-deficient RJK88.13 cells using Lipofectamine 2000 (Invitrogen, Carlsbad, CA) following the manufacturer's instructions. Stable transfectants were selected in medium lacking thymidine and containing 5 µM dipyridamole, a nucleoside transport inhibitor, to block the thymidine salvage

Table 1: Crystallographic Data and Refinement Statistics for Val3 Mutant Structures

	cocrystallized V3F	cocrystallized V3L	cocrystallized V3Y
X-ray source	APS SER-CAT 22ID	APS SER-CAT 22ID	APS SER-CAT 22ID
wavelength (Å)	1.00000	1.00000	1.00000
space group	$C2$	$P3_121$	$C2$
unit cell dimensions			
a (Å)	157.43	96.349	157.56
b (Å)	94.64	96.349	94.86
c (Å)	131.99	83.56	130.86
resolution range (Å) (highest-resolution shell)	44.0−2.75 (2.85−2.75)	50.00−3.0 (3.11−3.0)	50.00−2.75 (2.85−2.75)
mosaicity (deg)	0.86	0.48	1.5
completeness (%) (highest-resolution shell)	78.5 (26.4)	75.5 (22.6)	88.2 (67.0)
total linear R_{merge}	0.085	0.195	0.086
no. of reflections observed	33960	6685	36191
$I/\langle\sigma(I)\rangle$	15.5	5.3	13.5
redundancy (highest-resolution shell)	2.9 (1.2)	2.5 (1.1)	1.6 (1.4)
rmsd for bonds (Å)	0.009	0.012	0.053
rmsd for angles (deg)	1.5	2.3	4.4
Ramachandran statistics			
residues in most favored regions	753 (78.1%)	161 (72.2%)	704 (73.2%)
residues in additionally allowed regions	210 (21.8%)	59 (26.5%)	257 (26.7%)
residues in generaously allowed regions	1 (0.1%)	3 (1.3%)	1 (0.1%)
residues in disallowed regions	0	0	0
R	0.232 (CNS)	0.252 (CNS)	0.237 (CNS)
R_{free}	0.258 (CNS)	0.298 (CNS)	0.254 (CNS)

	V3L (high salt)	V3F (high salt)	V3T (high salt)	V3Y (high salt)
X-ray source	APS SER-CAT 22ID	APS SER-CAT 22ID	APS SER-CAT 22ID	APS SER-CAT 22BM
wavelength (Å)	1.00000	1.00000	1.00000	1.00000
space group	$P3_121$	$P3_121$	$P3_121$	$P3_121$
unit cell dimensions				
a (Å)	95.546	96.022	95.616	95.70
b (Å)	95.546	96.022	95.616	95.70
c (Å)	80.932	80.723	81.616	81.94
resolution range (Å) (highest-resolution shell)	50.0−1.56 (1.62−1.56)	50.0−1.75 (1.81−1.75)	50−2.050 (2.12−2.05)	37.0−1.86 (1.93−1.86)
mosaicity (deg)	0.26	0.83	0.29	0.19
completeness (%) (highest-resolution shell)	86.8 (54.4)	86.0 (45.4)	95.2 (76.5)	91.6 (57.5)
total linear R_{merge}	0.062	0.084	0.063	0.061
no. of reflections observed	53034	37576	26097	33719
$I/\langle\sigma(I)\rangle$	16.1	11.6	17.7	35.5
redundancy (highest-resolution shell)	11.2 (3.2)	4.9 (2.0)	5.4 (5.1)	5.1 (2.1)
rmsd for bonds (Å)	0.017	0.027	0.006	0.023
rmsd for angles (deg)	1.6	2.3	1.2	2.0
Ramachandran statistics				
residues in most favored regions	210 (89.0%)	204 (89.1%)	109 (87.6%)	189 (88.7%)
residues in additionally allowed regions	24 (10.2%)	24 (10.5%)	26 (12.0%)	22 (10.3%)
residues in generaously allowed regions	2 (0.8%)	1 (0.4%)	1 (0.5%)	2 (0.9%)
residues in disallowed regions	0	0	0	0
R (%)	0.209 (Refmac)	0.217 (Refmac)	0.201 (Refmac)	0.230 (Refmac)
R_{free} (%)	0.233 (Refmac)	0.253 (Refmac)	0.235 (Refmac)	0.268 (Refmac)

pathway. Stable transfectants were pooled together and grown in a mass culture.

Cell-Free Extracts. To prepare bacterial protein extracts, TX61 cells containing mutated pTS080 plasmids were inoculated into 5−10 mL of LB containing 50 μg/mL tetracycline and grown overnight at 37 °C. Cells in exponential growth were collected by centrifugation, resuspended in 300 μL of buffer A [50 mM Tris-HCl (pH 7.4), 1 mM EDTA, and 14 mM β-ME] and sonicated using a Biosonik iV sonicator (Bronwill, Rochester, NY). The sonicated cells were centrifuged at 13000g and 4 °C for 10 min. The supernatant was separated from the cell debris.

To prepare extracts from stably transfected RJK88.13 cells, cells were split into 60 mm plates and cycloheximide (50 μg/mL) was added after 24 h. Cells were harvested at the indicated time points and lysed by sonication (3 × 10 s) in NET2 buffer [50 mM

Tris-HCl (pH 7.4), 150 mM NaCl, and 0.05% Nonidet P-40] containing 10 mM dithiothreitol (DTT), 2 mM β-mercaptoethanol, 5 mM phenylmethanesulfonyl fluoride (PMSF), 200 μg/mL aprotinin, 100 μg/mL pepstatin, and 50 μg/mL leupeptin. The crude lysates were centrifuged at 17000g for 1 h at 4 °C, and the supernatant was separated from the cell debris. Total protein from all extracts was quantified using the Bradford Bio-Rad assay reagent (*18*) with bovine serum albumin as the standard.

Western Blotting. Total protein (15−50 μg per lane) was separated by electrophoresis in 12% SDS−PAGE gels and transferred to an Immobilon-P PVDF membrane (Millipore, Bedford, MA) in buffer containing 25 mM Tris base, 192 mM glycine, and 20% methanol with a Bio-Rad Trans-Blot SD apparatus (Bio-Rad, Hercules, CA). For immunodetection, standard procedures were employed. Cross-reacting protein

was detected as described previously (*19*) by utilizing the murine anti-human TS monoclonal antibody, D3B31 (1:1000 dilution in TBS-T), as the primary antibody; goat anti-murine monoclonal antibody conjugated to horseradish peroxidase (1:2500 dilution in TBS-T) as the secondary antibody (Bio-Rad); and lumigen PS-3 acridan (ECL Plus, Amersham Pharmacia Biotech, Piscataway, NJ) as the horseradish peroxidase (HPR) substrate. The HPR reaction was visualized by chemiluminescence and autoradiography. Autoradiographs were digitized by scanning at 600 dpi using a Hewlett-Packard C4100 scanner. Protein levels were analyzed by densitometry using an Odyssey Infrared Imaging System (LI-COR, Lincoln, NE) or with ImageJ (National Institutes of Health, Bethesda, MD).

Analysis of Growth Rates. For qualitative analysis, TX61$^-$ cells transformed with pTS080 constructs were streaked on agar-minimal medium plates in the presence or absence of 100 μg/mL thymidine overnight at 37 °C. For quantitative analysis, transformants were incubated overnight at 37 °C in minimal medium (*20*), supplemented with 100 μg/mL thymidine, 25 μg/mL kanamycin, and 10 μg/mL tetracycline. The cultures were diluted 1:100 into minimal medium with or without 100 μg/mL thymidine and supplemented with 25 μg/mL kanamycin and 10 μg/mL tetracycline. The cultures were incubated at 37 °C, and optical densities were determined using a Klett-Summerson colorimeter with a green filter over a 9 h period. Untransformed TX61$^-$ cells were used as a negative control.

Expression and Purification of Recombinant Human TS Enzymes. The recombinant proteins were purified as described previously (*17*).

Enzyme Kinetics. Enzyme activity was measured spectrophotometrically by monitoring the absorbance change accompanying the conversion of mTHF to DHF ($\varepsilon_{340} = 6.4$ mM^{-1} cm^{-1}) using a Shimadzu UV 1601 spectrophotometer (Shimadzu Corp.). Measurements were taken at 37 °C in buffer A. One unit of enzyme activity is defined as the amount of enzyme required to synthesize 1 μmol of thymidylate per minute. For determination of kinetic constants for dUMP, initial velocities were measured by utilizing 40 nM purified protein, 0.15 mM mTHF, and dUMP concentrations ranging from 25 μM to values between 100 and 400 μM. The reaction mixture, dUMP and buffer A, was preincubated for 3 min at 37 °C prior to addition of enzyme, immediately followed by addition of the mixture to a prewarmed cuvette containing mTHF. Data presented are averaged from three independent determinations. Kinetic constants were determined by fitting the data by nonlinear least-squares analysis to the hyperbolic form of the Michaelis−Menten rate equation using KaleidaGraph WIN (version 3.6x, Synergy Software, Reading, PA).

Crystallization. High-salt crystals of four Val3 mutants were grown using the hanging drop method in high-ammonium sulfate (AS) conditions as described previously (*3*). Briefly, 100 mM Tris base (pH 8.5), 20 mM BME (2-mercaptoethanol), and 32−40% ammonium sulfate (AS) were used.

For cocrystallization experiments, the proteins were incubated with 2 mM dUMP or FdUMP overnight and then separated from excess ligand with Sephadex G-50-80 gel filtration (Sigma). The final protein concentrations were 8.0, 4.5, and 6.5 mg/mL, for V3L, V3F, and V3Y, respectively. V3L low-salt crystals were grown in 100 mM Tris base (pH 8.5), 20 mM BME, 30 mM AS, and 16% polyethylene glycol (PEG) 4000. V3F low-salt crystals were grown in 100 mM Tris base (pH 8.0), 20 mM BME, 30 mM AS, and 24% PEG 4000. V3Y low-salt crystals were grown in
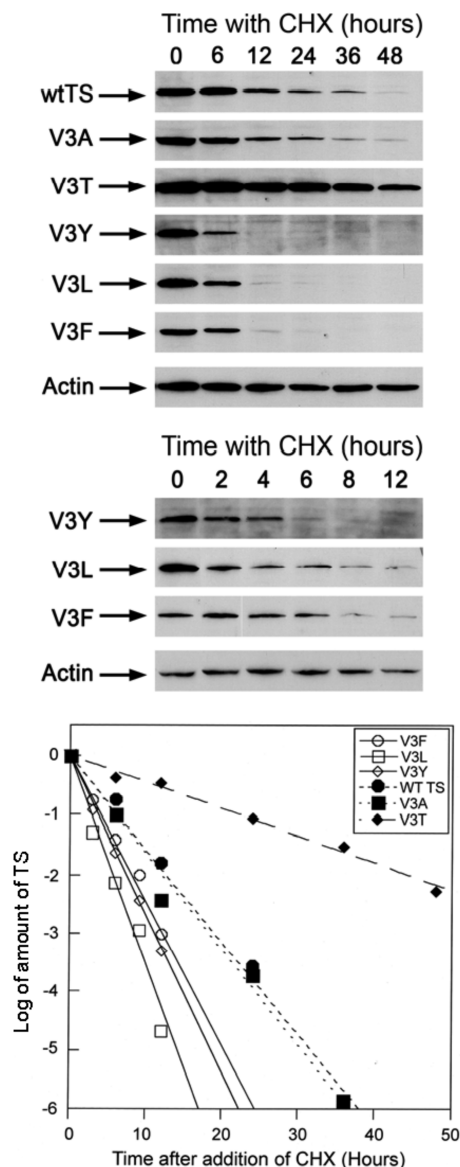

FIGURE 1: Intracellular stability of wild type hTS and mutants with substitutions at Val3. Stably transfected cells were treated with cycloheximide at the indicated time points, and TS levels were analyzed by immunoblotting using an anti-human TS monoclonal antibody (D3B31). Blots were stripped and reprobed with actin as an internal control to normalize quantitation using ImageJ. Half-lives were determined from the shown log$_2$ plots of hTS levels (normalized vs the actin content in each lane) determined by densitometry. The top panel shows Western blot analyses of wt and Val3 mutant hTS protein levels after treatment with cycoheximide (CHX) for 0, 6, 12, 24, 36, and 48 h. The middle panel shows Western blot analyses of V3Y, V3L, and V3F mutants after treatment with CHX for 0, 2, 4, 6, 8, and 12 h. The bottom panel shows a log$_2$ plot of the relative amount of protein in the band for hTS (each unit corresponds to one-half-life) for wt and Val3 mutants after treatment with CHX at the indicated time points.

100 mM Tris base (pH 8.0), 20 mM BME, 30 mM AS, and 24% PEG 4000. Crystals were transferred to artificial mother liquor additionally containing 20% ethylene glycol and flash-frozen in liquid nitrogen vapors.

X-ray Diffraction Data Collection and Structure Determination. Data were collected on the ID22 or BM22 beamline at Argonne National Laboratory and processed with HKL2000 (*21*). Data collection and processing statistics are listed in Table 1. The high-AS structures of V3T, V3F, and V3L were determined

using molecular replacement with CNS (*22*) using the hTS structure (PDB entry 1YPV) as the search model. The crystal structure of cocrystallized V3F was determined with AMoRe (*23*) from the CCP4 suite of programs (*24*) using the R163K structure (PDB entry 2RD8), which represents the active conformer (*25*), as the starting model. The crystal structures of V3L and V3Y under low-salt conditions were determined by molecular replacement to compensate for slightly different unit cell dimensions using the V3F structure as the starting model. Structure rebuilding and subsequent refinements were performed using Turbo-Frodo (*26*) and CNS, respectively. The final refinements of the high-AS structures were conducted using Refmac5 (*27*), and the final refinements of low-salt structures were performed using CNS. Superpositions were calculated using LSQKAB (*28*) from the CCP4 suite of programs. Figures 2, 3, and 5 were prepared using Turbo-Frodo. Figure 4 was made using MOLSCRIPT (*29*) and Raster3D (*30*). *R* factors of the final models are listed in Table 1 along with data collection and other refinement statistics.

RESULTS

Growth Analysis of Bacterial Transformants. TX61⁻ cells lack TS protein due to insertional disruption of the thyA
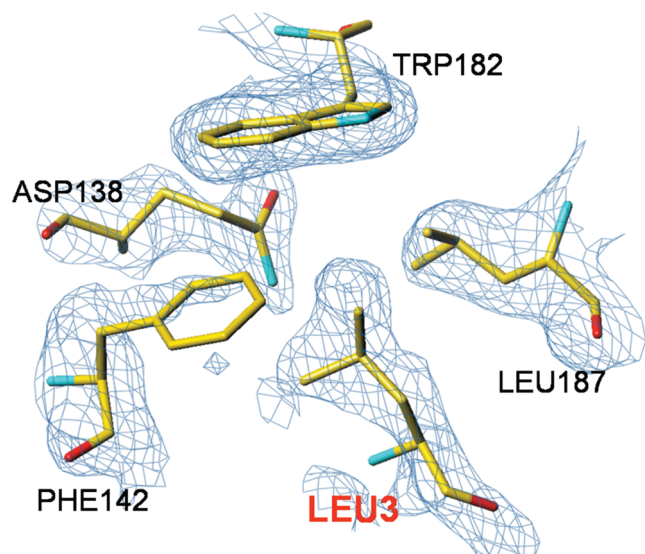

FIGURE 2: Stabilization of the inactive conformation in V3L. The $2F_o - F_c$ electron density map is contoured at the 1σ level. There is a likely leucine residue, labeled Leu3, interacting with loop 181−197 in the inactive conformation.

gene (*15*). To grow, the cells must be provided with exogenous thymidine or transformed with a plasmid construct expressing a functional TS. All hTS mutants constructed provided sufficient TS activity to support the growth of TX61⁻ cells as indicated by the formation of colonies in medium lacking thymidine. In contrast, untransformed TX61⁻ cells failed to grow in the thymidine deficient medium. The growth rates of TX61⁻ transformed with wild-type and mutant TSs in minimal medium lacking thymidine compared to untransformed TX61⁻ cells (in the presence of thymidine) are shown in Figure 1 of the Supporting Information. The growth rates of all mutants were similar except for that of V3A which exhibited an extended lag phase and a slight decrease in growth rate. Cell-free extracts from all transformants were analyzed by Western blotting (Figure 2 of the Supporting Information). The data appear to indicate that the decreased rate of growth of V3A is not due to its significantly lower level of expression compared to those of the other mutants.

Intracellular Protein Stability. To determine the effects of mutations at Val3 on intracellular protein stability, we stably transfected TS-deficient Chinese hamster lung cells (RJK88.13) with plasmid pJZ205 expressing wt hTS or the various mutant forms of hTS. All mutants were capable of supporting the growth of these cells in the absence of exogenous thymidine and in the presence of the nucleoside transport inhibitor, dipyridamole, providing the basis for selection of stably transfected cells. The cultured cells were treated with cycloheximide to stop protein synthesis, and steady-state levels of wt and mutant hTS proteins were determined by immunoblotting at the indicated time points after cycloheximide addition. The results presented in Figure 1 show that, with the exception of V3A, Val3 substitutions have strong effects on the half-lives of the TS proteins. wt TS and V3A had half-lives of approximately 6 h, while the V3T mutant had a half-life of approximately 24 h. In contrast, V3Y, V3L, and V3F were less stable and had half-lives of 2.5, 2.5, and 3.5 h, respectively (Figure 1). Sequence-based analysis using Terminator (*31*) very strongly predicts that all Val3 mutants, like wt hTS, have a free Pro2 at the N-terminus.

Steady-State Kinetic Properties. Kinetic parameters of mutants were analyzed under conditions in which the concentration of mTHF is fixed at 5-fold the K_m value for wt hTS. The resulting $k_{m,app}$ for dUMP and V[dUMP] are listed in Table 2. In general, the values of $K_{m,app}$ are higher and V[dUMP] lower for the mutant enzymes. Most mutants are only modestly impaired; however, V3F and V3L have $K_{m,app}$ values that are higher by factors of 58 and 47, respectively, relative to that of wt hTS. The
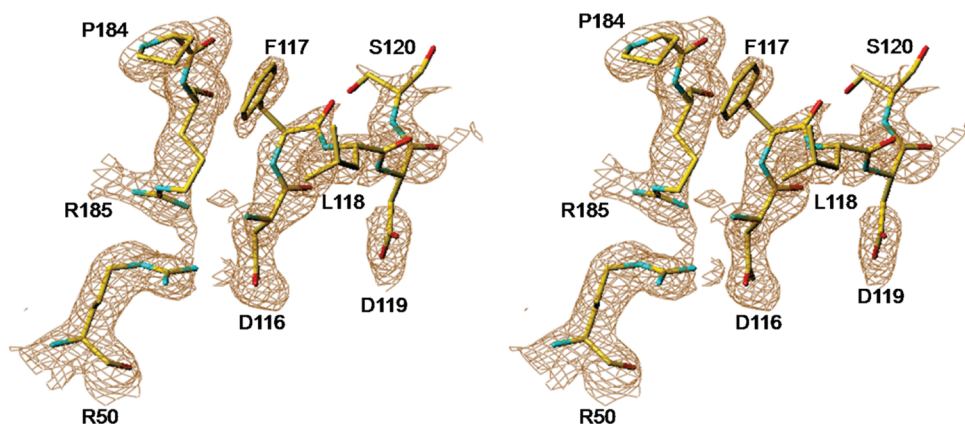
FIGURE 3: Stereoview of a fragment of the new conformation of loop 116−120 observed in the high-salt V3L structure.

variation in *V*[dUMP] values is much lower, and all mutants are at least half as active as the wild-type enzyme.

Crystal Structures. All crystals obtained at high AS concentrations (1.3−1.6 M) have excellent scattering power; the V3L diffraction to 1.6 Å resolution is the best ever reported for hTS, likely through additional stabilization of the inactive conformation (vide infra). Forms of loop 181−197 are in the inactive conformation, as expected, since this conformation is stabilized by sulfate ions. The high-AS structure of V3L showed well-defined electron density at the site at which a *tert*-butyl group was observed previously (*13*). This density, shown in Figure 2, corresponds to a leucine rather than a valine. The distance between Pro26, the first residue observed at the N-terminus, and the putative Leu3 is 43 Å, which is approximately half of the length of 23 residues in an extended conformation. No evidence of a bound moiety of any type in this site was observed in the other structures reported here. The electron density for a fragment of loop 100−130 is shown in Figure 3. The loop, which is disordered in other structures containing loop 181−197 in the inactive conformation, was mostly observed (only residues from position 104 to 108 are missing). This clearly eliminates Leu118

or Leu121 as a possible ligand in the hydrophobic pocket at Trp182 and Leu187. Interestingly, the conformation of this loop in the high-AS structure of V3L is somewhat different from that observed in the active conformation (shown in Figure 4). In the high-AS structures of V3F, this new conformation of the loop was also observed.

Perhaps due to the high resolution of the data, a previously unidentified piece of density close to the catalytic site was also observed. It likely represents a partially occupied peptide chain for which the sequence could not be identified; consequently, a polyalanine model was fitted to the density (shown in Figure 3 of the Supporting Information). No non-protein polymers were present in the crystallization medium. This polyalanine fragment can be seen in all the inactive structures of the Val3 mutants obtained under high-salt conditions. The disordered C-terminus, residues 310−313, and loop 104−108 are too short to generate this density, leaving only the N-terminus, residues 1−25, as a possible source. Alternatively, the density may arise from a noncovalently bound proteolytic fragment. The conformations of loops and the new fragments from all structures are summarized in Table 3.

The crystals obtained under low-AS conditions had significantly less scattering power than those obtained under high-AS conditions; consequently, only their major features are discussed. In the V3L structure, the inactive conformation was observed, and there was no bound nucleotide, even though the enzyme was incubated with dUMP prior to crystallization. In contrast, V3F cocrystallized with FdUMP under low-salt conditions, yielding the enzyme in the active conformation. One subunit from the dimer binds FdUMP, and the other binds a sulfate ion, reflecting the reported negative cooperativity of the enzyme. The FdUMP binding mode is, however, different from that previously observed for nucleotides. While the phosphate group binds in the
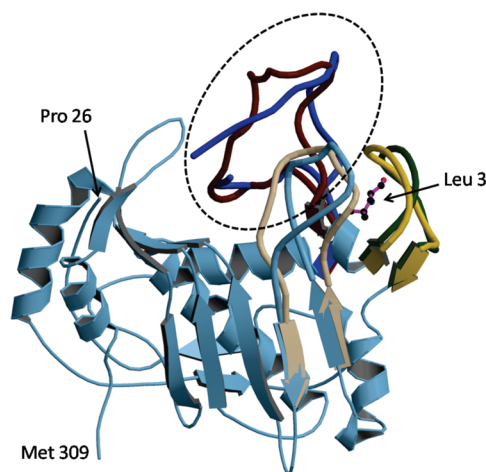

FIGURE 4: Comparison of loops in V3L hTS, which is in an inactive conformation, with loops from hTS in the active conformation (from the hTS·dUMP·raltitraxed inhibitory complex, PDB entry 1HVY). Loop 100−130 is colored dark blue (V3L) and brown (complex) and is highlighted by the oval. Loop 144−154 is colored dark green in V3L and orange in the complex. Loop 181−197, which contains the catalytic Cys195, is shown in the active conformation (from the complex) colored gray and in the inactive conformation (from V3L) colored light blue which is also used for the constant part of the molecule.
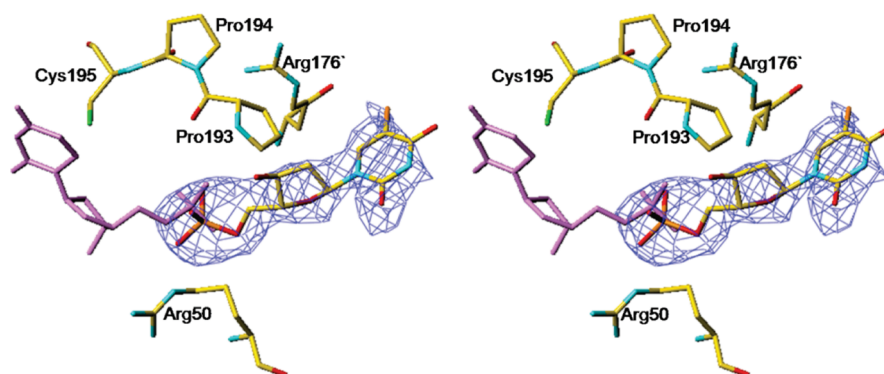
Table 2: Steady-State Kinetic Constants for Wild-Type hTS and hTS Mutants at Position 3[a]

hTS	V (s^{-1})	$K_{m,app}$ (μM)	V/K_m (s^{-1} μM^{-1})
wild type	3.04 ± 0.02	2.3 ± 0.2	1.3
V3A	0.96 ± 0.05	22 ± 5	4.3×10^{-2}
V3F	1.6 ± 0.3	134 ± 6	1.2×10^{-2}
V3L	2.6 ± 0.2	109 ± 2	2.4×10^{-2}
V3T	1.8 ± 0.1	11 ± 3	0.17
V3Y	2.6 ± 0.1	4.4 ± 0.2	0.60

[a]The dUMP concentration was varied from 25 to 400 μM.

FIGURE 5: Stereoview of the FdUMP binding site in the V3F complex. Omit electron density is contoured at the 1σ level. Colored purple is the superposition, based on Cα positions, of dUMP bound in the hTS·dUMP·raltiterxed inhibitory complex (*10*).

Table 3: Summary of Loop Conformations and Observed Ligands in Crystal Structures

	high-salt unliganded structures				low-salt cocrystallization structures		
	V3L hs	V3F hs	V3Y hs	V3T hs	V3L with dUMP	V3F with FdUMP	V3Y with FdUMP
ligand present	Leu3	no	no	no	no	FdUMP	no
loop 180−198	inactive	inactive	inactive	inactive	inactive	active	active
loop 109−130	new conformation	new conformation	disordered	disordered	disordered	active conformation	active conformation
polyalanine	yes	yes	yes	yes	no	no	no
space group	$P3_121$	$P3_121$	$P3_121$	$P3_121$	$P3_121$	C_2	C_2
resolution (Å)	1.56	1.75	1.86	2.05	3.0	2.75	2.75

standard site, the uridylate moiety is pointed in an opposite direction (shown in Figure 5). V3Y also cocrystallized with FdUMP under low-AS conditions, yielding the enzyme in the active conformation. However, the density for FdUMP is not clear, indicative of disorder; consequently, only a sulfate ion was modeled in each subunit. This likely reflects a low propensity of V3Y for nucleotide binding in the unique mode observed for V3F, as indicated by the disparate $K_{m,app}$ values.

DISCUSSION

The prevailing opinion about the N-terminal extension is that it has nonenzymatic functions. This hypothesis is supported by the poor sequence conservation of this region, including the most drastic difference, a complete lack of the extension in prokaryotes. The results reported here do not challenge this view. Rather, they indicate that such extensions can easily interact with the catalytic site of the enzyme and affect its enzymatic properties. Such interactions need not be strong and specific to be significant due to a high local concentration resulting from its covalent attachment. Therefore, the extensions are apparently under evolutionary pressure to achieve their physiological function without affecting other parts of the enzyme.

For all mutants studied here, the values of V[dUMP]$_t$ are only slightly reduced, indicating that after substrate binding occurs, the catalytic machinery is essentially unaffected by the Val3 substitutions. The $K_{m,app}$ values in some mutants are, however, quite different, especially for a variant residue that is not directly involved in substrate binding. In the hTS·dUMP·raltitrexed inhibitory complex, which should be a good model for the catalytic complex, dUMP is sequestered from the solvent, and it is highly unlikely that the N-terminus, which is disordered, interacts directly with the substrate (*11*). For the two mutants that stand out in terms of significantly increased $K_{m,app}$ values, the mechanisms by which the dUMP binding is affected appear to be entirely different. For V3L, the equilibrium between the active and inactive conformations of loop 181−197 and the conformation of loop 100−130 appear to be affected. It is surprising that the effects of a very conservative change, V3L, are so large. They likely are related to enhanced binding of the Leu3 side chain in the hydrophobic pocket formed by loop 181−197. If so, small molecules binding in this pocket should function as allosteric inhibitors stabilizing the inactive conformer. Potential advantages of such inhibitors versus active site-directed inhibitors have been discussed (*3*, *32*).

Like V3L, V3F has strongly compromised dUMP binding. In the high-salt V3F structure, no density is observed in the hydrophobic pocket at loop 181−197, indicating that the mechanism through which $K_{m,app}$ is increased is different. The structure of the V3F·FdUMP complex suggests that the alternative mode of nucleotide binding, which uses a part of the active site and is thus inhibitory, is responsible for this effect. Again, this complex may be used as a starting point for the structure-based development of a new class of inhibitors. Despite these differences, V3L and V3F have a common structural feature: the conformation of the 109−130 module. This region is ordered, and its conformation is different from that observed in the active conformation of wt hTS (Figure 4). In the inactive conformer of native wt hTS and in V3Y and V3T, this module is disordered. It is likely that the disorder is due to a mixture of conformations observed in the active conformation and that observed in V3L and V3F.

The N-terminus of hTS has been shown to be an important structural determinant that controls protein turnover in mammalian cells. Deletions of six amino acids, or as few as one, result in stabilization of the enzyme with up to 5-fold increases in half-life (*8*, *9*). In addition, insertions at the N-terminus and certain substitutions at the penultimate proline residue of TS result in enzyme stabilization (*9*) due to posttranslational modifications by N^α-acetylation (*7*) that may block entry into the proteasomal core for degradation. The altered turnover rates of Val3 mutants confirm the role of the N-terminus and show that a residue in position 3 is almost as important as that in position 2. The observed variability among the mutants demonstrates the difficulty in pinpointing structure−function relationships. The relatively conservative substitution in V3T slowed intracellular degradation by a factor of 4. Three other substitutions studied here, including V3Y, which also introduces a hydroxyl function, had opposite effects, and one substitution had no effect. Among 21 mammalian TS molecules that have been sequenced, only four have Val at position 3. Ala3 is the most common, being found in 14 species; two have Thr3, and one has His3 (*7*). Thus, none of mutants for which we observed lower stability has been reported in mammalian cells.

TS enzymes from *E. coli* and the majority of other bacteria have catalytic efficiencies similar to those of mammalian enzymes despite lacking the N-terminal extension. Moreover, the extension is only poorly conserved in mammals. These observations suggested that the extension evolved to serve in roles that are not related to catalysis. Indeed, mutational analyses of the hTS N-terminus indicate that it plays a critical role in determining the intracellular stability by targeting the protein for degradation by the ubiquitin-independent proteasomal degradation pathway (*7−9*). This function is accomplished by maintaining an intrinsic disorder in the N-terminus rather than by sequence conservation (*7*). The studies of Val3 mutants indicate that, in addition to this role, the N-terminus may also affect the catalytic machinery of hTS, likely by altering conformational equilibria in this highly flexible protein and suggesting that variability in the N-terminus may affect a range of molecular properties. The studies of Val3 mutants reveal new conformational states of hTS and show

correlations between eukaryotic inserts and the N-terminus. Since these regions of the molecule are only poorly conserved, the ongoing efforts to generate inhibitors of TS that are species-specific (*33*) gain additional credibility.

ACKNOWLEDGMENT

SUPPORTING INFORMATION AVAILABLE

Growth curves for the mutants, images of SDS−PAGE gels, activity measurements as a function of dUMP concentrations, and stereoview of the polyalanine fragment from the V3F structure. This material is available free of charge via the Internet at http://pubs.acs.org.

REFERENCES

1. Humphreys, G. K., and Greenberg, D. M. (1958) Studies on the conversion of deoxyuridylic acid to thymidylic acid by a soluble extract from rat thymus. *Arch. Biochem. Biophys. 78*, 275–287.
2. Carreras, C. W., and Santi, D. V. (1995) The catalytic mechanism and structure of thymidylate synthase. *Annu. Rev. Biochem. 64*, 721–762.
3. Phan, J., Steadman, D. J., Koli, S., Ding, W. C., Minor, W., Dunlap, R. B., Berger, S. H., and Lebioda, L. (2001) Structure of human thymidylate synthase suggests advantages of chemotherapy with noncompetitive inhibitors. *J. Biol. Chem. 276*, 14170–14177.
4. Schiffer, C. A., Clifton, I. J., Davisson, V. J., Santi, D. V., and Stroud, R. M. (1995) Crystal structure of thymidylate synthase: A structural mechanism for guiding substrates into the active site. *Biochemistry 34*, 16279–16287.
5. Sotelo-Mundo, R. R., Ciesla, J., Dzik, J. M., Rode, W., Maley, F., Maley, G. F., Hardy, L. W., and Montfort, W. R. (1999) Crystal structures of rat thymidylate synthase inhibited by Tomudex, a potent anticancer drug. *Biochemistry 38*, 1087–1094.
6. Phan, J., Koli, S., Minor, W., Dunlap, R. B., Berger, S. H., and Lebioda, L. (2001) Human thymidylate synthase is in the closed conformation when complexed with dUMP and Raltitrexed, an antifolate drug. *Biochemistry 40*, 1897–1902.
7. Peña, M. M. O., Melo, S. P., Xing, Y., White, K., Barbour, K., and Berger, F. G. B. (2009) The intrinsically disordered N-terminal domain of thymidylate synthase targets the enzyme to the ubiquitin-independent proteasomal degradation pathway. *J. Biol. Chem. 284*, 31597–31607.
8. Pena, M. M. O., Xing, Y. Y., Koli, S., and Berger, F. G. (2006) Role of N-terminal residues in the ubiquitin-independent degradation of human thymidylate synthase. *Biochem. J. 394*, 355–363.
9. Forsthoefel, A. M., Pena, M. M. O., Xing, Y. Y., Rafique, Z., and Berger, F. G. (2004) Structural determinants for the intracellular degradation of human thymidylate synthase. *Biochemistry 43*, 1972–1979.
10. Shimizu, K., Ayusawa, D., Takeishi, K., and Seno, T. (1985) Purification and NH_2-terminal amino acid sequence of human thymidylate synthase in an overproducing transformant of mouse FM3A cells. *J. Biochem. 97*, 845–850.
11. Phan, J., Koli, S., Minor, W., Dunlap, R. B., Berger, S. H., and Lebioda, L. (2001) Human thymidylate synthase is in the closed conformation when complexed with dUMP and raltitrexed, an antifolate drug. *Biochemistry 40*, 1897–1902.
12. Schiffer, C. A., Davisson, V. J., Santi, D. V., and Stroud, R. M. (1991) Crystallization of human thymidylate synthase. *J. Mol. Biol. 219*, 161–163.
13. Lovelace, L. L., Minor, W., and Lebioda, L. (2005) Structure of human thymidylate synthase under low-salt conditions. *Acta Crystallogr. D61*, 622–627.
14. Almog, R., Waddling, C. A., Maley, F., Maley, G. F., and Van Roey, P. (2001) Crystal structure of a deletion mutant of human thymidylate synthase Δ(7−29) and its ternary complex with Tomudex and dUMP. *Protein Sci. 10*, 988–996.
15. Dev, I. K., Yates, B. B., Leong, J., and Dallas, W. S. (1988) Functional role of cysteine-146 in *Escherichia coli* thymidylate synthase. *Proc. Natl. Acad. Sci. U.S.A. 85*, 1472–1476.
16. Dev, I. K., Dallas, W. S., Ferone, R., Hanlon, M., McKee, D. D., and Yates, B. B. (1994) Mode of binding of folate analogs to thymidylate synthase: Evidence for a 2 asymmetric but interactive substrate-binding sites. *J. Biol. Chem. 269*, 1873–1882.
17. Lovelace, L. L., Johnson, S. R., Gibson, L. M., Bell, B. J., Berger, S. H., and Lebioda, L. (2009) Variants of human thymidylate synthase with loop 181−197 stabilized in the inactive conformation. *Protein Sci. 18*, 1628–1636.
18. Bradford, M. M. (1976) A rapid and sensitive method for the quantitation of microgram quantities of protein utilizing the principle of protein-dye binding. *Anal. Biochem. 72*, 248–254.
19. Steadman, D. J., Zhao, P.-S., Spencer, H. T., Dunlap, R. B., and Berger, S. H. (1998) A structural role for glutamine 214 in human thymidylate synthase. *Biochemistry 37*, 7089–7095.
20. Williams, A. W., Dunlap, R. B., and Berger, S. H. (1998) A hydroxyl group at residue 216 is essential for catalysis by human thymidylate synthase. *Biochemistry 37*, 7096–7102.
21. Otwinowski, Z., and Minor, W. (1997) Processing of X-ray diffraction data collected in oscillation mode. *Methods Enzymol. 276*, 307–326.
22. Brunger, A. T., Adams, P. D., Clore, G. M., Delano, W. L., Gros, P., Grosse-Kunstleve, R. W., Jiang, J. S., Kuszewski, J., Nilges, M., Pannu, N. S., Read, R. J., Rice, L. M., Simonson, T., and Warren, G. L. (1998) Crystallography and NMR system: A new software suite for macromolecular structure determination. *Acta Crystallogr. D54*, 905–921.
23. Navaza, J. (1994) AMoRe: An automated package for molecular replacement. *Acta Crystallogr. D50*, 157–163.
24. Collaborative Computational Project, Number 4 (1994) The CCP4 suite: Programs for protein crystallography. *Acta Crystallogr. D50*, 760–763.
25. Gibson, L. M., Lovelace, L. L., and Lebioda, L. (2008) The R163K mutant of human thymidylate synthase is stabilized in an active conformation: Asymmetry and reactivity of Cys195. *Biochemistry 47*, 4636–4643.
26. Roussel, A., and Cambillau, C. (1991) "Turbo Frodo" Silicon Graphics Geometry Partners Directory, pp 86, Silicon Graphics, Mountain View, CA.
27. Murshudov, G. N., Vagin, A. A., and Dodson, E. J. (1997) Refinement of Macromolecular Structures by the Maximum-Likelihood method. *Acta Crystallogr. D53*, 240–255.
28. Kabsch, W. (1976) A solution for the best rotation to relate two sets of vectors. *Acta Crystallogr. A32*, 922–923.
29. Kraulis, P. J. (1991) MOLSCRIPT: A program to produce both detailed and schematic plots of protein structures. *J. Appl. Crystallogr. 24*, 946–950.
30. Merritt, E. A., and Bacon, D. J. (1997) Raster3D: Photorealistic molecular graphics. *Methods Enzymol. 277*, 505–524.
31. Meinnel, T., Peynot, P., and Giglione, C. (2005) Processed N-termini of mature proteins in higher eukaryotes and their major contribution to dynamic proteomics. *Biochimie 87*, 701–712.
32. Berger, S. H., Berger, F. G., and Lebioda, L. (2004) Effects of ligand binding and conformational switching on intracellular stability of human thymidylate synthase. *Biochim. Biophys. Acta 1696*, 15–22.
33. Ferrari, S., Losasso, V., and Costi, M. P. (2008) Sequence-Based Identification of Specific Drug Target Regions in the Thymidylate Synthase Enzyme Family. *ChemMedChem 3*, 392–401.